JOURNAL OF MATERIALS SCIENCE **34** (1999) 2997–3006

Microstructural evolution of titanium nitride (TiN) coatings produced by reactive ion beam-assisted, electron beam physical vapor deposition (RIBA, EB-PVD)

D. E. WOLFE, J. SINGH
Applied Research Laboratory, The Pennsylvania State University, State College, PA 16804, USA
E-mail: jxs46@psu.edu

Titanium nitride (TiN) coatings have been successfully deposited on 304 stainless steel substrates by reactive ion beam-assisted, electron beam-physical vapor deposition (RIBA, EB-PVD). The hardness values of the TiN coatings varied from 800 to 2500 VHN depending on the processing condition. The lattice parameter and hardness variation were correlated with processing parameters such as: deposition rate, bias, ion source energies, process gas, substrate temperature, and coating composition. The hardness of the TiN coatings increased with increasing ion energy. The ion energies combined with the deposition rate were the limiting factors controlling the degree of surface texturing. Surface texturing was only observed for those coatings deposited >8 Å/s.

1. Introduction

The performance of cutting tools is restricted by their surface properties and thermal stability which can be enhanced by applying hard wear-resistant coatings. The properties of these coatings are often determined by their microstructure which is a function of the processing parameters. Tailoring the microstructure of coatings can lead to significant improvements in cutting tool life (greater than 500%) [1–3].

Hardness measurements are often used in characterizing wear-resistant coatings. Typically, a higher coating hardness value correlates to a better wear-resistance. The hardness of a coating is a function of composition, density, and texturing; all of which can be controlled during processing. Generally, coatings with high density are harder than those that are less dense (i.e., higher amounts of porosity). The use of ion beam assisted deposition increases coating density by adding additional energy to the system which increases surface mobility.

The use of titanium nitride as a coating material for high-speed steel cutting tools has been around for several decades. The hard TiN coating increases tool life by as much as tenfold [1]. The properties that make TiN an attractive coating for the tool industry are: high hardness [5–8], low coefficient of friction [4], good chemical/thermal stability [7–9], good adhesion, and good corrosion resistance [10]. The main property is its hardness, which results from the high degree of metallic and covalent bonding. TiN gets its strength from the small separation of atoms, large surface energy, and high elastic modulus (50×10^6 psi). The other physical properties that result in TiN being one of the most widely used commercial wear-resistant coatings are: high yield stress (2.0×10^6 psi), high specific gravity (5.4 g/cm^3), and high melting point (2950 °C) [11–26].

The performance of TiN coatings depends on its microstructural features that are often dictated by the coating process. TiN coatings are currently applied by various techniques: including chemical vapor deposition (CVD) [3, 27–29], physical vapor deposition (PVD) [30–35], ion implantation [10, 36, 37], ion plating [38, 39], and ion beam assisted deposition [40–43]. Details of these coating processes are discussed elsewhere [44–46]. The objective of this work was to improve the hardness and wear resistance of TiN coatings by altering the microstructure of the coating.

2. Experimental

TiN coatings were produced by reactive ion beam assisted, electron beam-physical vapor deposition (RIBA, EB-PVD) using a Denton (model #DV-SJ/26) evaporation system [46]. Prior to the deposition of TiN, titanium metal (99.999% purity-Cerac) pieces (size $\sim 6 \times 6$ mm) were vacuum melted to form a large ingot. This was done to prevent trapped gases from causing spitting during the evaporation process. 304 stainless steel substrates $1'' \times 1'' \times 0.30''$ were mounted at a distance of $9.75''$ above the source material. Prior to the TiN deposition, the substrates were sputter-cleaned by ionized argon gas.

The substrates were pre-heated using resistance heating to temperatures between 400 and 650 °C for

TABLE I Major processing parameters for titanium nitride (TiN) deposited by RIBA, EB-PVD

Sample number	T1	T2	T3	T4	T5	T6	T7	T8	T9	T10
Substrate temperature (°C)	400	600	600	600	600	600	600	650	650	650
Current density (μA/cm^2)	190	190	190	48	130	190	190	130	190	190
Bias voltage (V)	0	0	0	0	0	−100	−100	−100	−100	0

30 minutes. Nitrogen gas was flown into the ion source where it was ionized and directed towards the substrate. A 10 kV electron beam gun was used to simultaneously evaporate the titanium metal. The substrate temperature, ion current density, and bias were all varied as listed in Table I.

After depositing the TiN coating, a hardness evaluation of the coated samples was accomplished by using Vicker's hardness tests. A diamond indentor with an applied load of 20 g was used to measure the hardness of the coatings. Ten measurements were made on each of the samples with the average value being reported. The coated samples were sectioned using a low-speed diamond cutting saw to preserve the coating integrity. The morphology of the coated samples was examined by a JOEL field emission scanning electron microscope (SEM).

To determine the TiN coating thickness, profilometry experiments were also performed. Using a Philips X'Pert two-circle X-ray diffractometer, diffraction patterns were obtained to determine the lattice parameter and coating structure. The coatings were also characterized by electron probe microanalysis (EPMA) to determine the approximate compositions of the films.

3. Results and discussion

3.1. Hardness (VHN)

The hardness measurements of the various TiN coatings deposited on 304 series stainless steel plates by RIBA, EB-PVD are shown in Fig. 1. Since the coating thicknesses were relatively thin (1–10 μm), it was difficult to measure the hardness of the coating alone. The hardness values may be the resultant of the coating and the substrate.

The hardness of the TiN coatings varied from 800 to 2500 VHN and the color of the coatings changed correspondingly from dark-brown to gold. Sample T4 showed the lowest hardness of 800 VHN (a dull, dark brownish color), whereas Sample T9 had the highest hardness of ∼2500 VHN (a yellowish-gold color).

A few generalizations can be drawn from the hardness results and correlated with the processing parameters. The average hardness of the coatings with the applied bias (T6–T9) were relatively higher than those samples without bias (T1–T5, T10). It is believed that the bias resulted in a denser microstructure and thus, the higher hardness value. This finding supports those reported in the literature [1, 2, 5, 9, 14, 17, 47].

Hardness variation in the coating was correlated with the energy of the ion source. Fig. 2 shows the average Vicker's hardness (VHN) vs. current density (μA/cm^2) for Samples T3–T5. The general trend shows that the hardness of the coatings dramatically increased from 800 to 1800 VHN with increasing current density (40 μA/cm^2 to 130 μA/cm^2). There was no significant improvement in the hardness values by further increasing the current density above 130 μA/cm^2. The increase in hardness is probably the result of texturing and a more dense coating as discussed in the next section.

3.2. Electron probe microanalysis (EPMA)

The color of TiN coatings depends upon such factors as thickness, texturing, grain size, and the composition. The atomic percents of the titanium, nitrogen, and

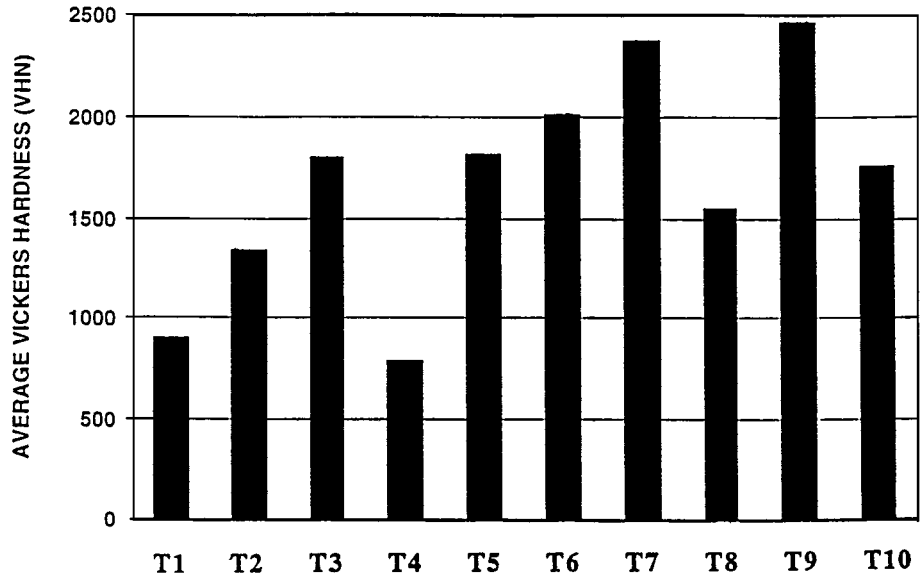

Figure 1 Average Vicker's hardness (VHN) of titanium nitride (TiN) deposited by RIBA, EB-PVD.

TABLE II The atomic percentages of titanium, nitrogen, and oxygen in the TiN coatings deposited by RIBA, EB-PVD

Samples number	Average atomic % titanium	Average atomic % oxygen	Average atomic % nitrogen	Titanium/nitrogen ratio	Color[a]	Average lattice parameter (Å)
T1	49.84	10.91	39.24	1.27	DBG	4.242
T2	48.51	4.89	46.60	1.04	LBG	4.241
T3	46.27	2.24	51.46	0.90	BBG	4.241
T4	47.42	7.33	45.25	1.05	DBG	4.241
T5	47.42	2.68	49.90	0.95	LBG	4.238
T6	49.02	6.37	44.60	1.10	MBG	4.241
T7	47.43	4.76	47.81	0.99	BBG	4.238
T8	45.94	3.81	50.26	0.91	BBG	4.234
T9	49.31	4.87	45.82	1.08	YG	4.241
T10	49.28	2.87	47.86	1.03	MBG	4.241

[a]DBG = Dark brownish-gold, LBG = Light brownish-gold, BBG = Bright brownish-gold, MBG = Medium brownish-gold, and YG = Yellowish-gold.

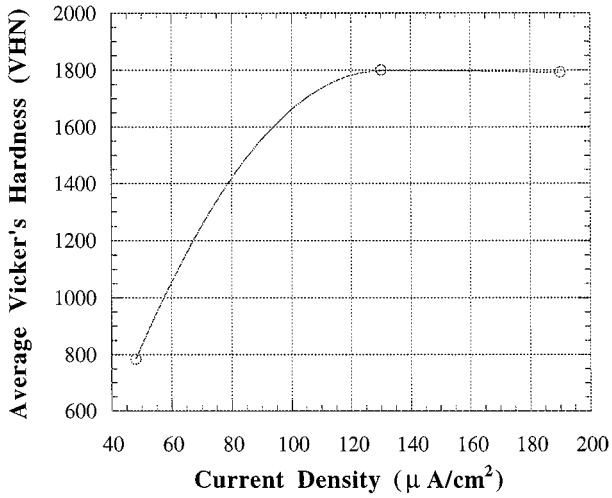

Figure 2 Average Vicker's hardness (VHN) vs. current density (μm/cm^2) for Samples T3–T5.

oxygen found in the bulk coatings were determined by electron probe microanalysis (EPMA), and are listed in Table II.

Sample T1 showed the largest titanium/nitrogen ratio of 1.27 as well as the highest percentage of oxygen (10.91%) in the coating. This data suggests that the film was deficient in nitrogen. The nitrogen deficiency, combined with the large amount of oxygen are most likely responsible for the dark brownish-gold color of the TiN film.

The variation of the oxygen in the TiN coatings can depend upon various factors including: (i) purity of the nitrogen gas, (ii) titanium purity, (iii) exposing the TiN coating to atmosphere at elevated temperatures, and (iv) the deposition temperature, microstructure (density), and evaporation rate. Oxidation of TiN was observed at very low temperatures ($<200\ ^\circ$C). The oxidation volume fraction in the TiN coatings depends upon the surface morphology and density that can be detected by EPMA (Table II). Coatings that contain high amounts of interconnected porosity and large gaps between the columnar microstructure are generally less dense. The large gaps between the columnar microstructure result in a larger surface area of the coating. When the coatings are exposed to the atmosphere, an oxide layer forms on the surface of the coating [48–53], and thus large amounts of oxygen are detected. There is a significant variation in the surface morphologies of the TiN coatings in Samples T1–T10; this could be one of the reasons for the variations in the oxide contents of the TiN-coated samples.

Sample T2 showed a closer Ti/N ratio of 1.04 with relatively low oxygen content of 4.89 at %. This finding was expected due to higher substrate temperature (600 $^\circ$C) and relatively low deposition rate (12.5 Å/s). It is believed that the lower deposition rate contributed to the denser coating, and thus a lower surface area (less surface oxidation).

Sample T3 contained approximately 2.24 at % oxygen with a Ti/N ratio of 0.90, which suggested that the sample was rich in nitrogen. The bright brownish-gold color observed for Sample T3 was a direct result of the relatively low oxygen content and dense surface. The lower deposition rate (3.7 Å/s) was probably the major processing parameter responsible for the higher hardness (1800 VHN) as compared with samples T1 (900 VHN) and T2 (1350 VHN).

Sample T5 resulted in a 0.95 Ti/N ratio with a low concentration of oxygen (2.68 at %). These values suggest that the coating contained high amounts of nitrogen. The low oxygen content in the TiN coating might be the result of better coating density. The light brownish-gold color of the coating was observed due to the combined effect of the low Ti/N ratio and the denser coating.

A negative bias was applied to Samples T6–T9. A negative bias generally results in a fine-grained, dense, microstructure similar to the IBAD process. By applying a negative potential to the substrate, positive species were accelerated towards the substrate's surface. These accelerated species impinge (bombard) on the growing film. The energy of these bombarding species is such that they create surface defects that lead to an increased number of nucleation sites, and thus produces a more dense, fine-grained microstructure [5, 9, 24].

Sample T8 showed a Ti/N ratio of 0.91 with an oxygen content of 3.81 at %, which is very similar to the results of Sample T5 (as expected). The color of the coating (Sample T8) appeared to be a bright brownish-gold color (similar to Sample T7). The major difference between Samples T8 and T5 was the -100 V bias applied to Sample T8 during deposition. In addition, the

substrate temperature was higher for T8 (650 °C) than for T5 (600 °C).

Sample T9 showed a Ti/N ratio of 1.08 with an oxygen content of 4.87 at %. This sample had the best yellowish-gold color of all of the samples, even though it was not stoichiometric. It appeared that the sample was deficient in nitrogen. The amount of nitrogen deficiency found within this sample was approximately the same amount of oxygen (4.8 at %) present in the film.

It was difficult to quantify the factors affecting the color of the TiN coatings since the color is dependent upon many factors including coating thickness, grain size, density, texture, and composition. Comparing Samples T3 to T4, the color of the coating changed from BBG to DBG as the oxygen content increased from 2.2 to 7.33% (Table II). The color of all the coatings with oxygen contents >7 wt % were DBG. It is interesting to note that the hardness increased as oxygen content decreased. This may be explained by the degree of surface oxidation and density (i.e., surface oxidation decreases with increasing density). For example, Samples T1 and T4 have low hardness values associated with high oxygen contents (10.9 and 7.33%, respectively). In contrast, Samples T3 and T5 have high hardness values (1800 VHN) with low oxygen contents 2.24% and 2.68%, respectively. Therefore, the hardness can be correlated with the composition, amount of surface oxidation, and thus density.

3.3. X-ray diffraction

X-ray diffraction was used to determine the structure and lattice parameters of the TiN coatings. The general accepted value for bulk TiN is 4.240 Å. However, the lattice parameter of thin films is expected to deviate from the bulk values as they are deposited under nonequilibrium conditions. As a result of the TiN coatings being thin, glancing angle (2θ-only) diffraction patterns were obtained to prevent diffraction from the underlying substrate.

The lattice parameters of Samples T1 to T10 ranged from 4.234 to 4.241 Å, which is expected as all of the films did not have stoichiometric compositions (Table II). In all of the samples, the X-ray diffraction results support the coatings being TiN as the diffracted peak positions matched those of the accepted stoichiometric TiN well within experimental error. Existence of the Ti_2N phase was not observed for T1–T10.

All of the TiN coatings deposited by RIBA, EB-PVD showed variation in the lattice parameters that were close to the stoichiometric value for TiN (4.240 Å). The small differences in the lattice parameters can be attributed to many factors as discussed below.

The chemical compositions of the coatings can affect the lattice parameter in several ways. Since TiN has a defect structure (titanium and nitrogen atoms are missing from the unit cell), excessive substitutional titanium or nitrogen atoms can cause changes in the lattice parameter (i.e., N (or Ti) atoms replace the Ti (or N) atoms in the atomic positions of the unit cell). Also, oxygen substitutional impurity atoms have been reported to result in a decreased lattice parameter [9].

Biasing causes stresses in the film (similar to IBAD), by the successive impingement of atoms on the surface of the depositing film which also affects the lattice parameter value [9]. In addition, interstitial nitrogen atoms generally result in an expansion of the lattice parameter. The high nitrogen to titanium ratios provide strong evidence of interstitial nitrogen. Interstitial nitrogen can result from a variety of factors including nonequilibrium growth conditions (low-substrate temperatures, high-bias voltages, and high-deposition rates) and ion beam-assisted deposition [9, 54–56].

Fig. 3a shows the X-ray diffraction pattern of Sample T4 with the maximum intensity corresponding to the (2 0 0) planes. The diffraction patterns of Samples T1, T2, and T8 also showed similar patterns with the (2 0 0) planes showing the maximum intensity.

The X-ray diffraction pattern of Sample T5 is shown in Fig. 3b. The higher degree of ion bombardment change the degree of texturing to the (111) planes. Similarly, Samples T7, T9, and T10 all show the (111) planes with the highest intensity.

With still higher ion bombardment (Sample T3 shown in Fig. 3c), the degree of texturing changed to the (2 2 0) planes. It is believed that the higher current densities provided additional energy to the system which enhanced the amount of surface mobility and allowed the low energy (fast growth) planes to survive.

From the diffraction patterns shown in Fig. 3a–c, the differences in intensities can be attributed to the degree of texturing in the coating produced by the use of the ion source during deposition. These results reconfirmed the previous finding that the use of ion beam-assisted deposition (IBAD) process can change the orientation of the growing film [58]. Therefore, by controlling the processing parameters, the degree of texturing and orientation of the coating can be controlled.

To ascertain a better understanding of the texturing occurring within the TiN coatings, pole figures were performed (discussed later) on four selected samples (T3–T5, and T9). Samples T3–T5 were selected because they were deposited under similar processing conditions, except with different ion beam energies that were believed to be the controlling factor in the texturing growth of the TiN coatings. Sample T9 was selected as it appeared to have the highest degree of texturing of all the deposited coatings.

3.4. Surface morphology

The surface morphology of the TiN coatings deposited by RIBA, EB-PVD were examined using scanning electron microscopy (SEM). Variation in the hardness values was correlated with the change in the surface morphology of the coated samples.

Fig. 4a shows the surface morphology of Sample T1. The average grain size of the TiN coating was in the range of 10–100 nm. The surface of the coating was not very dense. Voids/porosity in the surface of the coating were observed as marked by arrows in Fig. 4a. These voids most likely contributed to the low hardness value (900 VHN). The presence of voids and porosity is associated with the lower substrate temperature

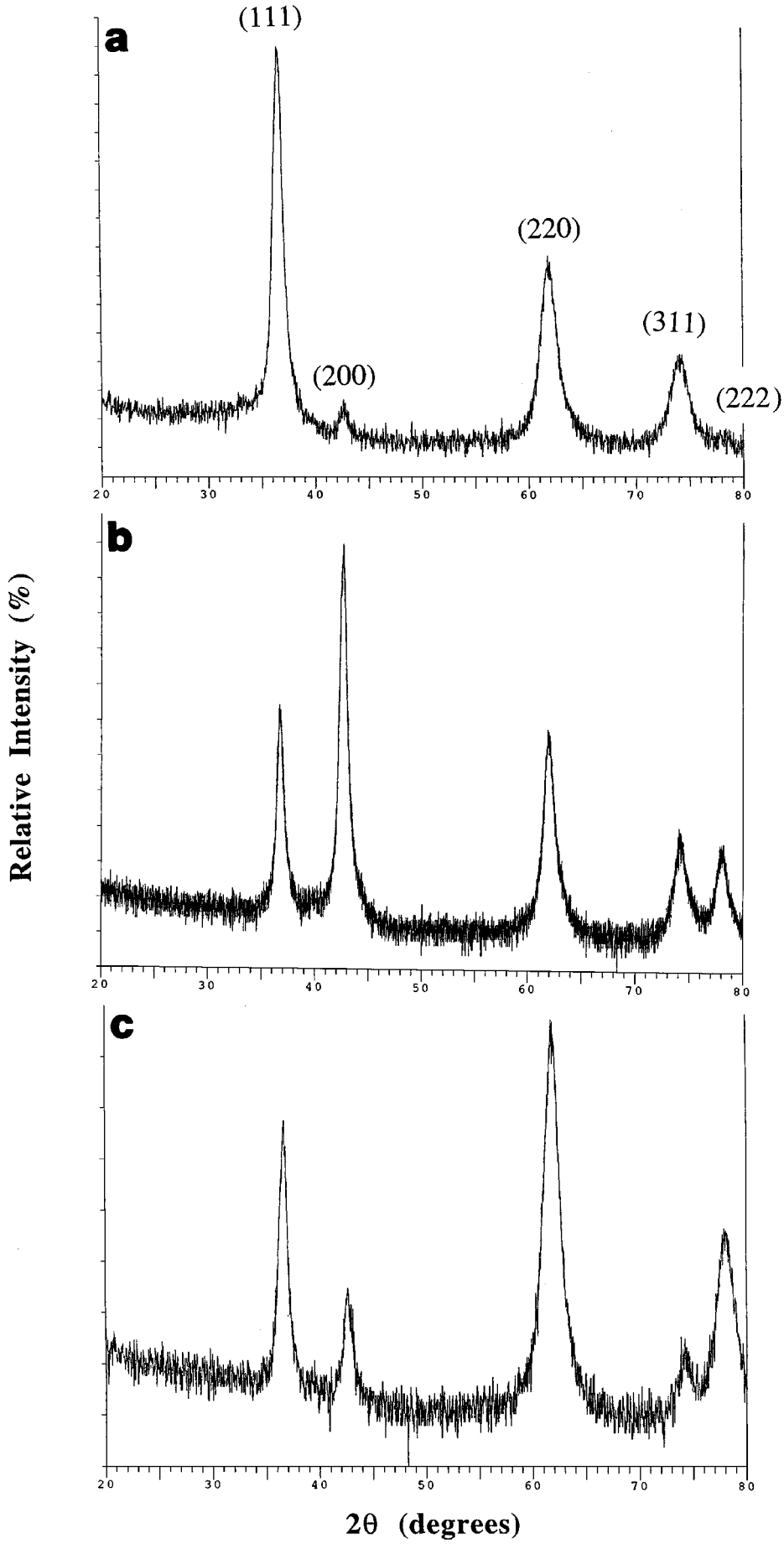

Figure 3 X-ray diffraction pattern showing the relative intensity (%) vs. 2θ (degrees) for Sample (a) T4, (b) T5, and (c) T3.

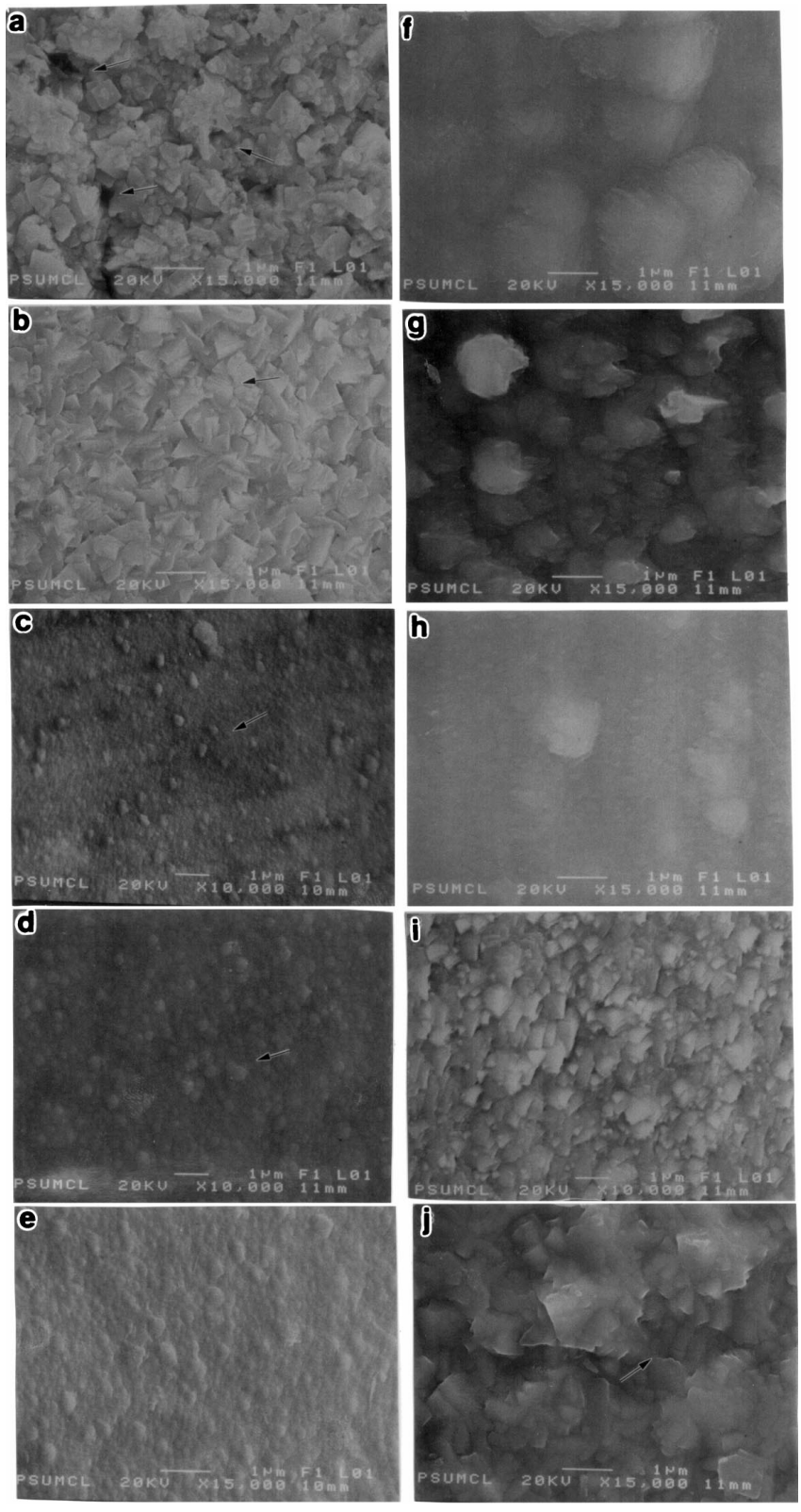

Figure 4 Scanning electron micrographs (SEM) showing the surface morphology of titanium nitride (TiN) deposited by RIBA, EB-PVD for Samples (a) T1, (b) T2, (c) T3, (d) T4, (e) T5, (f) T6, (g) T7, (h) T8, (i) T9, and (j) T10.

($T_s = 400\,^{\circ}$C), the high deposition rate (∼33 Å/s), and low adatom mobility of the species while condensing on the substrate. The voids/porosity in the coating are undesirable for better wear-resistant properties.

Sample T2 (Fig. 4b) shows a more dense titanium nitride coating with some texturing. Porosity and voids were not observed at the surface of the coating. High-magnification observations revealed a certain degree of texturing. The majority of the grains were submicron with a uniform size distribution. However, the presence of smaller grains (<100 nm) was still observed. The higher density was a result of the higher substrate temperature ($T_s = 600\,^{\circ}$C) combined with the lower deposition rate (12 Å/s). The denser coating also resulted in a higher hardness (1330 VHN) as compared with Sample T1 (900 VHN).

No evidence of surface texturing was observed for Sample T3 as shown in Fig. 4c. In addition, the grains

appeared to be more spherical. A small volume fraction of localized, larger grains (∼10%) were also observed throughout the surface of the film. These larger grains appeared to be randomly positioned and approximately 0.2 μm in size. The rest of the grains appeared to be much smaller than 100 nm. The high surface density and small grain size of the TiN coating contributed to the high hardness value (1800 VHN).

The surface morphology of Sample T4 (Fig. 4d) was similar to Sample T3 (Fig. 4b). Numerous defects were observed on the surface of the coating. These defects resulted in the low hardness value (800 VHN). These defects may have been due to nonuniform deposition in the coating. However, the grains appeared to have a more uniform size distribution (<0.5 μm) that is beneficial for wear-resistant applications.

A smaller volume fraction of surface defects (∼5%) were observed in the coating for Sample T5 (Fig. 4e) as compared to Sample T4. Even with the presence of these defects, the hardness of the coating was still high (1800 VHN), which is a typical hardness value (1800–2200 VHN) for stoichiometric, bulk TiN [9]. Evidence of surface texturing was not visible on the coated surface by SEM. It is important to mention here that even though surface texturing was not evident, growth texture was observed in the film by X-ray diffraction (Fig. 3b).

The surface morphology of Sample T6 appears to contain very few defects. Sample T6 (Fig. 4f) shows localized, small volume fraction of larger grains (1 to 2 μm in size) similar to Sample T3 (Fig. 4c). The TiN coating had a fine-grained microstructure (≤100 nm). This fine-grained microstructure probably contributed to the high hardness value (2000 VHN). Again, no evidence of surface texturing was observed.

The surface morphology of T7 appeared to be very dense with a uniform grain size (Fig. 4g). The grains appear to be approximately 1 μm in size. With the exception of a few growth defects, the film appears to have a dense, untextured surface.

Similarly to T3 and T6, the surface of Sample T8 (Fig. 4h) does not appear to be textured. However, X-ray diffraction showed a strong 200 orientation.

The surface morphology of Sample T9 (Fig. 4i) was similar to Sample T2 as surface texturing was observed. No porosity or voids were observed on the surface of the coating. The average grain size of the coating was in the submicron range (<0.5 μm). Thus, the combined effects of high surface density, fine-grained microstructure (<0.5 μm), and texturing resulted in a high hardness value (2500 VHN).

The surface morphology of Sample T10 (Fig. 4j) was similar to that of Samples T1, T2, and T9, but without any distinct texturing. The average grain size was less than 100 nm. This fine-grained microstructure might be the result of the higher deposition temperature (650 °C) and deposition rate (27 Å/s).

3.5. Processing trends for TiN by RIBA, EB-PVD

The major processing parameters that effected the quality of the titanium nitride coatings were: deposition rate, ion source energies (current and voltage), and negative biasing.

Samples T1, T2, T9, and T10 all showed evidence of surface texturing. Except for sample T6, it appeared that surface texturing of the TiN coatings only occurred when the deposition rate exceeded 10 Å/s. This finding was found to be independent of substrate temperature (400 °C, 600 °C, and 650 °C). This type of surface texturing can be explained by the degree of surface mobility at the substrate's surface. Generally, the substrate needs to be one half the melting point ($T_m = 0.5$) of the coating before a significant amount of surface mobility occurs. Surface texturing results when the coating condenses on the substrate's surface faster than the atoms can move to equilibrium lattice positions (low surface mobility). Under such deposition conditions, the slow-growth planes (1 1 1) may be surviving at the expense of the fast growth-planes (2 0 0 and 2 2 0). The additional energy (IBAD) etches the low-energy planes (2 0 0 and 2 2 0) which allows the high-energy planes to control the growth direction. Generally, low indexed planes (1 1 1) have a high lattice energy, and thus growth is slow [57]. The opposite is true for high indexed planes (2 0 0 and 2 2 0): low energy and fast growth. The use of IBAD (additional energy) suppresses the low-energy planes (2 0 0 and 2 2 0), which allows the high-energy planes to dominate.

In addition, the hardness of the coating increased when a negative bias was applied. It is believed that the negative bias created more surface defects, and thus an increased number of nucleation sites. The increased number of nucleation sites resulted in smaller grain sizes and thus, high density films.

3.6. Pole figure determination

Pole figures are receiving more attention as the orientation of the grains in thin films becomes more important. Qualitative as well as quantitative information can be obtained from pole figures. However, only a qualitative description of the texturing will be given to avoid confusion as pole figure theory is complex.

To better understand the degree of texturing in the coating, pole figures were obtained on three TiN-coated samples: T3 (high current density (190 μA/cm^2)), T4 (low current density (48 μA/cm^2)), and T5 (medium current density (130 μA/cm^2)). These samples were deposited under the same conditions but with different ion beam energies. The pole figures for Sample T9 were also obtained since the surface morphology of the SEM micrographs showed a high degree of surface texturing.

The pole figure for Sample T4 (48 μA/cm^2) is shown in Fig. 5. Weak texturing of the (1 1 1) planes was observed (Fig. 5a). This was supported by the low contour line intensities that were widely spaced. However, a slight degree of orientation/texture was observed for the (2 0 0) planes (Fig. 5b) oriented 45° from the normal to the surface. Similar to the (1 1 1) planes, the (2 2 0) planes showed weak texturing (Fig. 5a and c, respectively). A negligible amount of texturing was expected because of the low RIBAD energies.

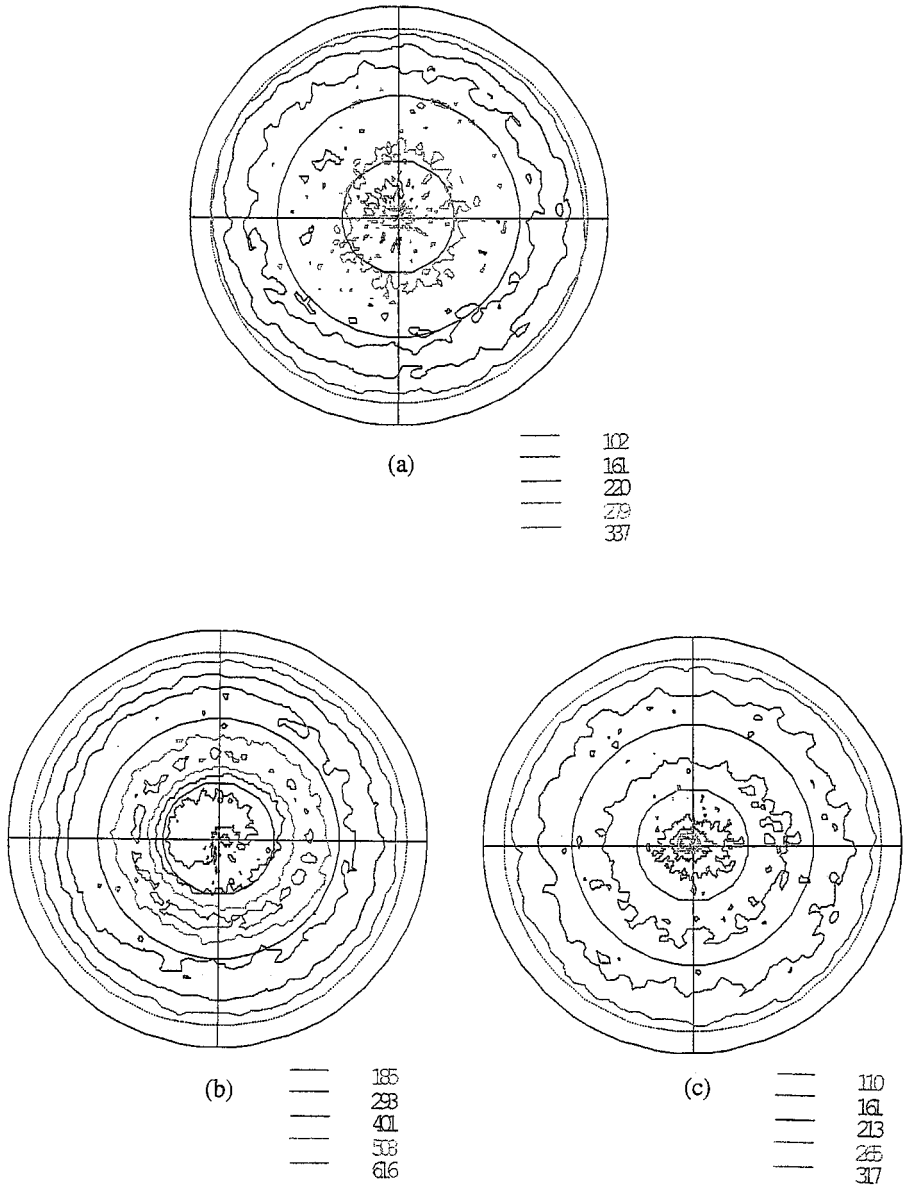

Figure 5 Pole figure data for Sample T4 showing the degree of texture for the (a) (1 1 1) planes, (b) (2 0 0) planes, and (c) (2 2 0) planes within the titanium nitride (TiN) coating.

The (1 1 1) planes of Sample T5 (130 μA/cm^2) showed medium texturing approximately 3–6 degrees from the center of the density map. This suggests that the columnar growth of the (1 1 1) planes within the grains did not grow exactly (parallel) to the surface of the substrate, rather grain growth was approximately 3–6 degrees to the surface. The (2 0 0) planes of T5 were more textured (approximately 57° from the surface of the coating) than those of T4. In addition, the (2 2 0) planes showed weak texturing 36° from the normal of the surface. The degree of texturing was much stronger for Sample T5 than Sample T4.

The highest degree of texturing was found in Sample T3 (190 μA/cm^2) which is consistent with the level of ion assist. The (1 1 1) planes of Sample T3 showed medium texturing. The (2 0 0) planes were strongly oriented 30° from the normal to the surface. In addition, the contour lines were closely spaced indicating strong textured growth of the (2 0 0) planes within the TiN coating. The (2 2 0) planes also showed weak texturing as the contour line intensities were low, and the contours were widely spaced.

Comparing Samples T3–T5, Sample T3 showed the highest degree of texturing, but not more than Sample T5. This is consistent with the hardness measurements showing very little improvement with increasing the current density above 130 μA/cm^2.

The high degree of surface texturing for Sample T9 (Fig. 6) was explained by the preferred orientation of certain planes within the TiN unit cell. Fig. 6a shows the pole figure for the (1 1 1) planes. It appeared that the (1 1 1) planes were oriented the strongest at an angle 44° from the normal to the surface. This orientation was strongly supported by the highly localized intensities and closely spaced contour lines. The (2 0 0) planes (Fig. 6b) were oriented 27° from the planes parallel to the surface as shown by the close contour line spacing and high contour intensity. In addition, contour lines of the (2 2 0) planes showed a high degree of intensity, suggesting a strong degree of texturing during film growth (Fig. 6c).

Unlike Samples T3–T5, all of the (1 1 1), (2 0 0), and (2 2 0) planes in Sample T9 showed a high degree of orientation. This high degree of grain orientation resulted

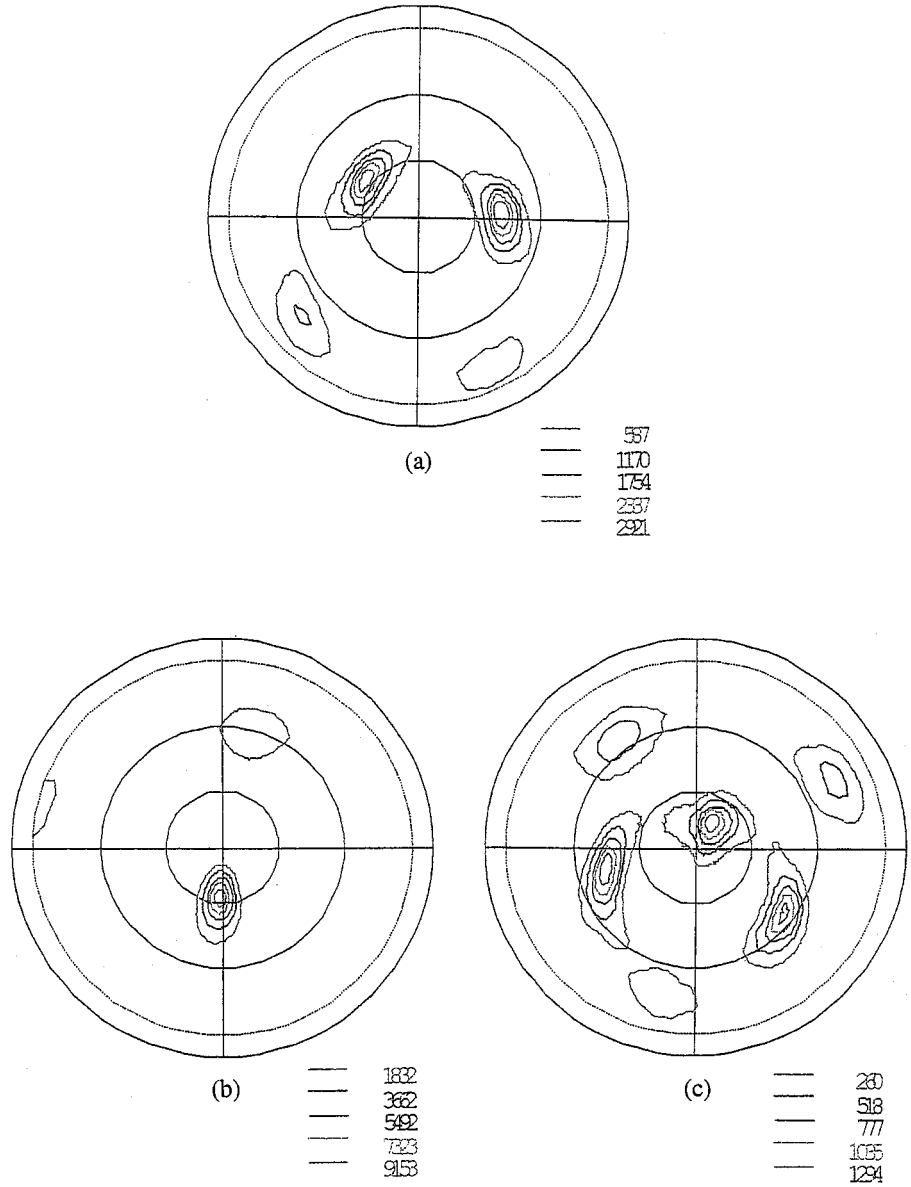

Figure 6 Pole figure data for Sample T9 showing the degree of texture for the (a) (1 1 1) planes, (b) (2 0 0) planes, and (c) (2 2 0) planes within the titanium nitride (TiN) coating.

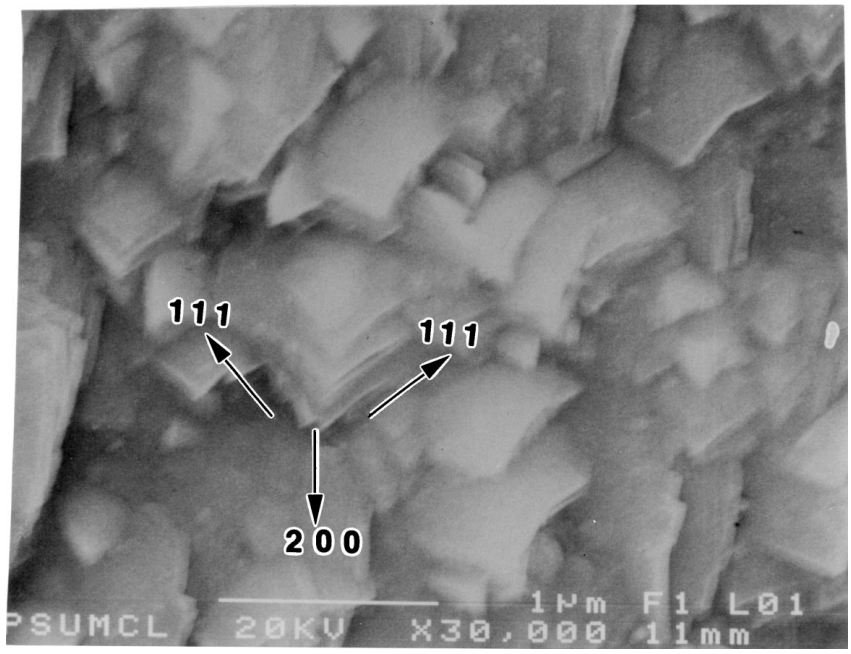

Figure 7 Scanning electron micrograph (SEM) showing the grain growth orientation as it relates to the textured surface morphology.

in the surface morphology being textured (Fig. 7). It appeared that the growth of the grains grew in the orientation as shown by the arrows in Fig. 7. These results correlate very well with the surface morphology and X-ray diffraction results.

4. Conclusions

Titanium nitride coatings were produced with hardness values ranging from 800 to 2500 VHN. Hardness increased proportionally with increasing ion current densities from 48–130 μA/cm^2. No significant changes in the hardness values were observed with further increasing the ion current densities (>130 μA/cm^2). Biasing the substrate increased the hardness of the coating. In addition, the use of the bias did not affect the surface morphology of the coatings. All of the TiN coatings deposited on 300 series stainless steel substrates showed evidence of growth texturing, but only selective films also showed surface texturing. Texturing in the TiN coating was observed as low as 400 °C on stainless steel substrates (300 series). Surface texturing was only obtained when the deposition rate exceeded 8 Å/s. The degree of growth texture and surface texturing was dependent on the energy of the ion source. Color variation of the coatings was the combined effect of the degree of texturing, surface oxidation, density, and thickness.

Acknowledgements

One of the authors (Douglas E. Wolfe) would like to extend his gratitude to Charles Brickell, Jr., Dale Donner, and the Applied Research Laboratory (ARL Penn State) for their help and financial support of this project.

References

1. R. HATSCHEK, *American Machinist* (1983) 129–144.
2. J. SUNDGREN, B. JOHANSSON and S. KARLSSON, *Thin Solid Films* **105** (1983) 353–366.
3. W. SPROUL, *Cutting Tool Engineering* (1994) 52–57.
4. D. MONAGHAN and K. LAING, *Finishing* **17**(11) (1993) 1–6.
5. J. SUNDGREN and L. HULTMAN, in "Materials and Processes for Surface and Interface Engineering," edited by Y. Pauleau (Kluwer Academic Publishers, Dordrecht, The Netherlands, 1995) pp. 453–474.
6. S. DIDZIULIS, J. LINCE, T. STEWART and E. EKLUND, *Inorg. Chem.* **33** (1994) 1979–1991.
7. A. DUNAND, H. FLACK and K. YVON, *Phys. Rev. B* **31**(4) (1985) 2299–2315.
8. P. BLAHA, J. REDINGER and K. SCHWARZ, *ibid.* **31**(4) (1985) 2316–2325.
9. J. SUNDGREN, *Thin Solid Films* **128** (1985) 45–55.
10. N. HEIDE and J. SCHULTZE, *Nuclear Instruments and Methods in Physic Research B* **80/81** (1993) 467–471.
11. R. JASCHEK and C. RUSSEL, *J. Non-Cryst. Solids* **135** (1991) 236–242.
12. Z. CHENG and J. ZHU, *J. Mater. Res.* **10**(4) (1995) 995–999.
13. W. ENSINGER, *Nuclear Instruments and Methods in Physics Research B* **80/81** (1993) 1409–1414.
14. Y. IGASAKI and H. MITSUHASHI, *Thin Solid Films* **70** (1980) 17–25.
15. W. SINKE, G. FRIJLINK and F. SARIS, *Appl. Phys. Lett.* **47**(5) (1985) 471–473.
16. S. SCHILLER, G. BEISTER and W. SIEBER, *Thin Solid Films* **111** (1984) 259–268.
17. J. POITEVIN and G. LEMPERIERE, *ibid.* **97** (1982) 69–77.
18. K. AHN, M. WITTMER and C. TING, *ibid.* **107** (1983) 45–54.
19. S. KANAMORI, *ibid.* **136** (1986) 215–227.
20. O. JOHANSEN, J. DONTJE and R. ZENNER, *ibid.* **153** (1987) 75–82.
21. G. HUBLER, D. VAN VECHTEN, E. DONOVAN and R. KANT, *Mat. Res. Soc. Symp. Proc.* **128** (1989) 55–60.
22. B. COLL, *Vide, Les Couches Minces* **261** (1992) 309.
23. D. NAGY, in "American Society of Mechanical Engineers, Applied Materials Division," edited by J. W. Wu (ASME, New York, 1992) pp. 1–7.
24. D. RICKERBY and P. BURNETT, *Science of Ceramics* **14**, 793–798.
25. R. CHOWDHURY, R. VISPUTE, K. JAGANNADHAM and J. NARAYAN, *J. Mater. Res.* **11**(6) (1996) 1458–1469.
26. T. WAKABAYASHI, J. WILLIAMS and I. HUTCHINGS, *Surface and Coatings Technology* **57** (1993) 183–189.
27. G. SANDHU, S. MEIKLE and T. DOAN, *Appl. Phys. Lett.* **63**(3) (1993) 240–242.
28. T. ARAI, H. FUJITA and K. OGURI, *Thin Solid Films* **165** (1988) 139–148.
29. B. KARLSSON, R. SHIMSHOCH, B. SERAPHIN and J. HAYGARTH, *Physica Scripta* **25** (1982) 775–779.
30. F. SEQUEDA, *J. Metals* (1986) 55–65.
31. J. STIMMELL, *J. Vac. Sci. Technol. B* **4**(6) (1986) 1377–1382.
32. T. BRAT, N. PARIKH, N. TSAI, A. SINHA, J. POOLE and C. WICKERSHAM, *ibid.* **5**(6) (1987) 1741–1747.
33. G. DIXIT, C. WEI, F. LIOU and H. ZHANG, *Appl. Phys. Lett.* **62**(4) (1993) 357–359.
34. S. ROHDE, Y. KIM and R. DEANGELIS, *J. Electronic Materials* **22**(11) (1993) 1327–1330.
35. G. MAH, P. MCLEOD and D. WILLIAMS, *J. Vac. Sci. Technol.* **11**(4) (1974) 663–665.
36. J. HIRVONEN, *Annu. Rev. Mater. Sci.* **19** (1989) 401–417.
37. G. WOLF, *J. Vac. Sci. Technol. A* **10**(4) (1992) 1757–1764.
38. D. MATTOX, *Electrochemical Technology* **2** (1964) 295–298.
39. W. MADER and H. FISCHMEISTER, *Thin Solid Films* **182** (1989) 141–152.
40. W. ENSINGER, R. EMMERICH and B. ENDERS, in "Surface Modification Technologies IV," edited by T. Sudarshan and D. Bhat (The Minerals, Metals & Materials Society, PA, 1993) pp. 859–880.
41. B. HAYWOOD, *Advanced Materials and Processes* **12** (1990) 35–40.
42. J. HIRVONEN, *Materials Science Reports* **6** (1991) 215–274.
43. Y. NAKAGAWA, S. OHTANI, T. NAKATA, MIKODA and T. TAKAGI, *Nuclear Instruments and Methods in Physics Research B* **80/81** (1993) 1402–1405.
44. R. BUNSHAH, "Handbook of Deposition Technologies for Films and Coatings" (Noyes Publications, Park Ridge, NJ, 1994).
45. M. HOCKING, "Metallic and Ceramic Coatings, Longman Scientific and Technical" (John Wiley & Sons Inc., 1989).
46. D. WOLFE, Thesis 1996mWolfe DE, Penn State Universiy, 1996.
47. S. YAMAMOTO and H. ICHIMURA, *J. Mater. Res.* **11**(5) (1996) 1149–1156.
48. H. TOMPKINS, *J. Appl. Phys.* **71** (1992) 980–983.
49. N. SAHA and H. TOMPKINS, *ibid.* **72** (1992) 3072–3079.
50. W. ENSINGER, *Nuclear Instruments and Methods in Physics Research B* **56/57** (1991) 648–651.
51. Y. SAKKA, S. OHNO and M. UDA, *J. Amer. Ceram. Soc.* **75**(1) (1992) 244–248.
52. H. TOMPKINS, *J. Appl. Phys.* **70** (1991) 3876–3880.
53. C. ERNSBERGER, J. NICKERSON and T. SMITH, *J. Vac. Sci. Technol. A* **4**(6) (1986) 2784–2788.
54. L. HULTMAN, G. HAKANSSON, U. WAHLSTROM and J. SUNDGREN, *Thin Solid Films* **205** (1991) 153–164.
55. J. ECHIGOYA and Z. LIU, *ibid.* **198** (1991) 293–300.
56. V. VALVODA, *J. Alloys and Compounds* **219** (1995) 83–87.
57. C. WILD, N. HERRES and P. KOIDL, *J. Appl. Phys.* **68**(3) (1990) 973–976.
58. M. KIUCHI, A. CHAYAHARA, Y. HORINO, K. FUJII, M. SATOU and W. ENSINGER, *Applied Surface Science* **60/61** (1992) 760–764.

Received 7 January 1997
and accepted 13 November 1998